

## Dynamics of adatoms on solid surfaces

L. Y. Chen and S. C. Ying

*Department of Physics, Brown University, Providence, Rhode Island 02912*

(Received 3 December 1993)

A microscopic theory for the diffusive and vibrational motion of adsorbed atoms on a solid surface is presented. We evaluate and analyze the dynamical structure factor and the velocity autocorrelation function. The quasielastic scattering peak in the dynamical structure factor is found to consist of mixed contributions from diffusive and vibrational motion. The vibrational peak indicates a shift and broadening from anharmonic effects and frictional damping. As the temperature is lowered the diffusion constant crosses over from a continuous Brownian motion behavior to a thermally activated Arrhenius form. When the frictional coefficient is varied at low temperatures, the diffusion constant crosses over smoothly from the multisite jumping regime at low friction, via the transition-state regime, to the high-friction overdamped regime. Applied to Na on the Cu(001) surface, our theoretical predictions on the quasielastic-peak width and the temperature dependence of the shift of the vibrational mode agree quantitatively with recent experimental measurements. For adatoms on anisotropic bcc (110) surfaces, we also study the diffusion anisotropy as well as the coupling of the two frustrated translational modes.

### I. INTRODUCTION

The diffusive motion of adsorbed atoms and their vibrational motion near the minima of the adsorption potential are usually studied as separate topics because they involve different length and time scales.<sup>1-8</sup> At low temperatures, the adatom spends most of its time vibrating rapidly around an adsorption-potential minimum and diffusion proceeds by thermally activated rare events of jumping from one adsorption site to another in its neighborhood. Information about the diffusive motion can be extracted from the quasielastic spectrum of the dynamic structure factor at small wave vectors whereas the adatom vibrational motion can be studied at finite frequencies. Indeed both these aspects have been successfully probed via He atom scattering studies.<sup>8</sup> There are however situations in which the two modes of motion become coupled and their effects are difficult to separate. The first is at temperatures higher than the diffusion barrier height, when the time spent by the adatom near the minima of the adsorption potential is comparable to the time in the in-between regions. The second situation is at larger wave vectors corresponding to motion of the adatom at smaller length scales. In the study of the quasielastic spectrum of the dynamic structure factor, the full width at half maximum (FWHM)  $\Delta E(\mathbf{q})$  contains the crucial information. It is usually assumed that its wave vector dependence can be modeled by a multisite jumping theory.<sup>5,9</sup> However, such a model neglects the vibrational motion of the adatom altogether and cannot describe  $\Delta E(\mathbf{q})$  properly at larger wave vectors. A scrutiny of the He scattering experimental data<sup>8</sup> indicates that this is indeed the situation. This suggests that the diffusive and vibrational motion both contribute to the quasielastic peak and are intimately coupled. This fact is particularly noticeable for a wave vector along a nonprincipal axis.

In this paper, we present a theoretical study of adatom dynamics in which diffusion and vibration are treated on

an equal footing. The motion of the adatom is restricted to two dimensions and hence vibrational motion normal to the surface is not included. In Sec. II, we outline the formalism developed previously<sup>10</sup> to evaluate various dynamic correlation functions. In Sec. III, we study the case of a separable potential with fourfold symmetry and evaluate the dynamic structure factor as well as the velocity autocorrelation functions. When the theory is applied to Na/Cu(001), the FWHM of the quasielastic scattering peak and the temperature-dependent vibrational frequency shift are both in quantitative agreement with recent experimental data.<sup>8</sup> Also presented in this section is the diffusion constant for a whole range of the frictional coefficient parameter  $\eta$  at various temperatures. As the frictional coefficient increases from  $\eta \ll \omega_0$  to  $\eta \gg \omega_0$ , the diffusion constant clearly indicates a smooth cross-over from the multiple-site jumping regime via the transition-state regime (where  $\eta \sim \omega_0$ ) to the high-friction overdamped regime. When the temperature is varied for a fixed value of the friction parameter, the diffusion constant crosses over from high-temperature behavior of Brownian motion in a continuous medium to the Arrhenius form of thermally activated jumping over barriers at low temperatures. In Sec. IV, we study anisotropic adsorption systems with nonseparable adsorption potential and evaluate the velocity autocorrelation function. Its zero-frequency limit gives directly the diffusion constant, whereas its finite-frequency part provides us with full information of the vibrational motion of the adatom. We then apply the formalism to adsorption on bcc (110) surfaces. The diffusive constants along the [001] and [110] directions possess temperature and friction dependence similar to that for surfaces with fourfold symmetry. Their ratio goes to the right geometric value at low temperatures as the diffusion proceeds predominantly by the thermally activated events of crossing the saddle points from a well to one of its neighbor wells. In this case, each jump has a projection of a distance  $a$  along the

[001] direction and  $\sqrt{2}a$  along  $[1\bar{1}0]$ . The anharmonicity-induced shift and broadening of the vibrational modes are particularly interesting because the bare frequencies of the two frustrated translational modes differ from each other. When they are coupled together via the anharmonicity of the adsorption potential, the line shift of the two modes exhibits a nonmonotonic temperature dependence. In Sec. V we present the concluding remarks. Preliminary results of some of the work have already been reported elsewhere.<sup>11,12</sup>

## II. FORMULATION

We start with a model Hamiltonian of the form

$$H = \frac{\mathbf{p}^2}{2m} + V(\mathbf{R}) + \sum_{\lambda} \mathbf{M}(\mathbf{R}, \lambda) \cdot \mathbf{u}_{\lambda} + H_{\text{ph}}. \quad (2.1)$$

Here  $m$ ,  $\mathbf{R}$ , and  $\mathbf{p}$  are, respectively, the mass, displacement vector, and momentum of the adatom.  $V(\mathbf{R})$  is the adsorption potential.  $\mathbf{u}_{\lambda}$  is the eigenvector for the  $\lambda$ th eigenmode of the substrate vibrational excitations, characterized by the harmonic Hamiltonian  $H_{\text{ph}}$ .<sup>13</sup> The scattering off substrate phonons results in an effective friction which plays a central role in the diffusion process and broadens the vibrational spectrum at very low temperatures. At temperatures of interest, the diffusion is mainly due to thermally activated jumping over barriers and the vibrational mode is broadened and shifted by the anharmonicity of the adsorption potential as well as by frictional damping.

In order to describe the motion of an adatom on surface, we calculate the dynamic structure factor defined as

$$S(\mathbf{q}, \omega) = \int dt e^{-i\omega t} \langle e^{-i\mathbf{q} \cdot \mathbf{R}(t)} e^{i\mathbf{q} \cdot \mathbf{R}} \rangle, \quad (2.2)$$

and the velocity autocorrelation function

$$\mathbf{D}(\omega) = \int dt e^{-i\omega t} \left\langle \frac{\mathbf{p}(t)}{m} \frac{\mathbf{p}}{m} \right\rangle, \quad (2.3)$$

where  $\mathbf{q}$  is the wave vector and the angle brackets stand for the thermal statistical average. While  $S(\mathbf{q}, \omega)$  contains all the information of quasielastic scattering spectra,

consisting of both the diffusive and vibrational contributions,  $\mathbf{D}(\omega=0)$  is directly the diffusion constant, and  $\mathbf{D}(\omega \sim \omega_0)$  demonstrates the shifting and broadening of the vibrational modes.

We have developed previously<sup>10</sup> a formalism for the evaluation of  $S(\mathbf{q}, \omega)$  and  $\mathbf{D}(\omega)$  based on the Mori projection-operator formalism.<sup>14</sup> Here we briefly summarize its main features important in the present discussion. In the Hilbert space consisting of all the dynamic variables of the adatom as vectors, the scalar product of two arbitrary variables  $A$  and  $B$  is defined as the thermal statistical average of their products, i.e.,  $\langle A | B \rangle = \langle A * B \rangle$ . The following set of vectors is complete in the subspace of the adatom's dynamics,

$$A_{mn}(\mathbf{K}) = h_m(p_x) e^{i(K_x + q_x)x} h_n(p_y) e^{i(K_y + q_y)y}, \quad (2.4)$$

where  $h_n(p) = 2^{-n/2} H_n(p/\sqrt{2mkT})$  and  $H_n$  are the usual Hermitian polynomials,  $m, n = 0, 1, 2, \dots$ .  $\mathbf{K}$  stands for a reciprocal lattice vector, and  $\mathbf{q}$  stands for an arbitrary wave vector within the first Brillouin zone. The norm matrix  $\chi = \langle A | A \rangle$ ,

$$\chi_{mn, m'n'}(\mathbf{K}, \mathbf{K}') = m!n! \delta_{mm'} \delta_{nn'} \rho(\mathbf{K} - \mathbf{K}'), \quad (2.5)$$

where  $\rho(\mathbf{K} - \mathbf{K}')$  is the Fourier transform of the density. The dynamic structure factor matrix,

$$\mathbf{C}_{mn, m'n'}(\mathbf{K}, \mathbf{K}', \omega) = \int dt e^{i\omega t} \langle A_{mn}(\mathbf{K}, t) | A_{m'n'}(\mathbf{K}') \rangle, \quad (2.6)$$

is determined by

$$\mathbf{C}(\omega) = \chi \cdot [-i\omega + \mathbf{b} + \Sigma(\omega)]^{-1}. \quad (2.7)$$

In Eq. (2.6),  $A_{mn}(\mathbf{K}, t) \equiv e^{-iL t} A_{mn}(\mathbf{K}, t)$  with  $L$  being the Liouville operator. Equation (2.7) is written in a matrix form where the indices  $m$ ,  $n$ , and  $\mathbf{K}$  are implicit. The vector  $\mathbf{q}$  however is fixed and not a part of the indices. Note that this equation reduces to that obtained by Wahnström in the Fokker-Planck equation approach<sup>15</sup> for the case of a one-dimensional adsorption potential. Here the matrix  $\mathbf{b} = \chi^{-1} \langle A | iL | A \rangle$  is block tridiagonal, namely,

$$\begin{aligned} \mathbf{b}_{mn, m'n'}(\mathbf{K}, \mathbf{K}') = & \sqrt{kT/m} \{ [\delta_{m, m'+1} \delta_{n, n'} + (m+1) \delta_{m, m'-1} \delta_{n, n'}] i(K_x + q_x) \delta_{\mathbf{K}, \mathbf{K}'} \\ & + [\delta_{m, m'} \delta_{n, n'+1} + (n+1) \delta_{m, m'} \delta_{n, n'-1}] i(K_y + q_y) \delta_{\mathbf{K}, \mathbf{K}'} \} \\ & + \frac{1}{\sqrt{mkT}} [\delta_{m, m'-1} \delta_{n, n'} i(K'_x - K_x) + \delta_{m, m'} \delta_{n, n'-1} i(K'_y - K_y)] V(\mathbf{K} - \mathbf{K}'). \end{aligned} \quad (2.8)$$

The memory function

$$\Sigma(\omega) = \chi^{-1} \int_0^{\infty} dt e^{i\omega t} \langle QL A | e^{-iQLQ t} | QL A \rangle. \quad (2.9)$$

Here  $Q$  is the projection operator out of the adatom subspace such that  $QB = B - A\chi^{-1} \langle A | B \rangle$ . Thus we obtain

$$QiL A_{m, n}(\mathbf{K}) = Q \left[ \dot{p}_x \frac{dh_m(p_x)}{dp_x} h_n(p_y) + \dot{p}_y \frac{dh_n(p_y)}{dp_y} h_m(p_x) \right] e^{i(K_x + q_x)x + i(K_y + q_y)y}. \quad (2.10)$$

Substituting Eq. (2.10) into Eq. (2.9) for the memory function and also making the approximation of replacing the projected Liouville operator  $QLQ$  simply by  $L$ , we arrive at the expression

$$\begin{aligned} \Sigma_{mn,m'n'}(\mathbf{K}, \mathbf{K}'; \omega) = & \frac{1}{m!n!} \sum_{\mathbf{K}_1} \rho^{-1}(\mathbf{K}, \mathbf{K}_1) \int_0^\infty dt e^{i\omega t} [ \langle Q\dot{p}_x(t) m A_{m-1,n}(\mathbf{K}_1, t) | Q\dot{p}_x m' A_{m'-1,n'}(\mathbf{K}') \rangle \\ & + \langle Q\dot{p}_y(t) n A_{m,n-1}(\mathbf{K}_1, t) | Q\dot{p}_y n' A_{m',n'-1}(\mathbf{K}') \rangle ] . \end{aligned} \quad (2.11)$$

As  $Q$  projects out all the regular part of the force  $\dot{\mathbf{p}}$  due to the adiabatic periodic adsorption potential, we have

$$Q\dot{\mathbf{p}} = \sum_{\lambda} \nabla[M(\mathbf{R}, \lambda) \cdot \mathbf{u}_{\lambda}] . \quad (2.12)$$

This is just the random force on the adatom due to coupling to substrate phonons. Further decoupling of the adatom variables  $\mathbf{p}$  and  $\mathbf{R}$  from the substrate variables  $\mathbf{u}_{\lambda}$  leads to the expression for the memory function,

$$\begin{aligned} \Sigma_{mn,m'n'}(\mathbf{K}, \mathbf{K}'; \omega) = & \frac{1}{m!n!} \sum_{\mathbf{K}_1} \rho^{-1}(\mathbf{K}, \mathbf{K}_1) \int_0^\infty dt e^{i\omega t} [ \eta_x(t) m m' C_{m-1,n,m'-1,n'}(\mathbf{K}_1, \mathbf{K}'; t) \\ & + \eta_y(t) n n' C_{m,n-1,m',n'-1}(\mathbf{K}_1, \mathbf{K}'; t) ] , \end{aligned} \quad (2.13)$$

where  $\eta_{\alpha}$  ( $\alpha = x$  or  $y$ ) is the diagonal element of the friction tensor given by the expression,

$$\eta(t) = \left\langle \sum_{\lambda} \nabla[M(\mathbf{R}, \lambda) \cdot \mathbf{u}_{\lambda}(t)] \middle| \sum_{\lambda} \nabla[M(\mathbf{R}, \lambda) \cdot \mathbf{u}_{\lambda}] \right\rangle . \quad (2.14)$$

Note that the friction function  $\eta_{\alpha}(t)$  is just the autocorrelation of the random force. With Eqs. (2.5), (2.8), and (2.14), Eqs. (2.7) and (2.13) constitute a closed set of matrix equations for the dynamic correlation functions that can be solved self-consistently. This is the so-called mode-mode coupling approximation. Results for specific parameters have been obtained within this approximation.<sup>11,15</sup>

When the motion of the adatom is on a time scale much longer than that for the substrate phonons, one can employ the initial value approximation (IVA),<sup>10,15</sup> namely, the adatom variable  $A(\mathbf{K}, t)$  in Eq. (2.11) can be simply replaced by  $A(\mathbf{K}, t=0)$ . Then the memory function simplifies to

$$\Sigma_{mn,m'n'}(\mathbf{K}, \mathbf{K}'; \omega) = \delta_{mm'} \delta_{nn'} \delta_{\mathbf{K}\mathbf{K}'} (\eta_x(\omega) m + \eta_y(\omega) n) , \quad (2.15)$$

and becomes diagonal in all the indices. In the remainder of this paper, we will concentrate our discussion on the IVA using the form (2.15) for the memory function. Besides the fact that it is quantitatively valid for slow diffusive motion and the frustrated translational modes of the adatom, most of the qualitative features we discuss here also survive in the full mode-mode coupling approximation.<sup>11</sup>

We give here an explicit expression for  $\eta_{\alpha}(\omega)$  using the three-dimensional Debye model for the substrate phonons and a simplified form for the coupling matrix element

$$\frac{\partial M^{\alpha}(\mathbf{R}, \lambda)}{\partial x_{\beta}} = A e^{i\mathbf{q}_{\lambda} \cdot \mathbf{R}} . \quad (2.16)$$

Here  $\mathbf{q}_{\lambda}$  is the wave vector for the  $\lambda$ th phonon mode. In this simplified model

$$\eta_{\alpha}(\omega) = \eta \left[ \theta(\omega_D - \omega) - \frac{i}{2\pi} \ln \left| \frac{\omega - \omega_D}{\omega + \omega_D} \right| \right] , \quad (2.17)$$

with

$$\eta = \frac{3|A|^2}{4\pi m c^3} \frac{1}{\rho} . \quad (2.18)$$

Here  $\omega_D$  is the Debye frequency,  $c$  the velocity of sound, and  $\rho = M/V$ , the mass density of the substrate. Obviously, the IVA is quantitatively valid when  $\omega_D$  is much higher than the frequency of the frustrated translational modes. Although only the coupling to substrate phonons is explicitly included in our model, the coupling to other substrate excitations such as electron-hole pairs can be included in a similar fashion. Since the electronic motion is on a much faster time scale than the typical diffusional or vibrational time, the IVA is an excellent approximation for this situation. In fact, the corresponding contribution to the memory function would be similar to that given by Eq. (2.17) with details only differing in the imaginary part, in addition to the fact that  $\omega_D$  would be replaced by the frequency scale appropriate for the electron-hole pair excitation, namely, the plasmon frequency. When we are concerned with the region  $\omega \ll \omega_D$  and  $\text{Im}\Sigma$  does not play a significant role, we can regard  $\eta$  as an effective friction which contains the effect of coupling of the adatom to all substrate excitations (electronic and vibrational).

We note that  $\chi$  is block diagonal and  $\Sigma$  is completely diagonal. The matrix  $\mathbf{b}$  is tridiagonal in  $(m+n)$ , the sum of the  $x$  index  $m$  and the  $y$  index  $n$ . Thus it is convenient to introduce a new index  $L = m+n$  and to label the matrix elements in  $(L, n)$ . Arranging the elements in blocks by  $L$ ,

$$\mathbf{b} = [\mathbf{b}_{L,L'}] , \quad (2.19)$$

where  $L, L' = 0, 1, 2, \dots$ ; it is tridiagonal,

$$\mathbf{b} = \begin{pmatrix} 0 & \mathbf{b}_{0,1} & 0 & 0 & \cdots \\ \mathbf{b}_{1,0} & 0 & \mathbf{b}_{1,2} & 0 & \cdots \\ 0 & \mathbf{b}_{2,1} & 0 & \mathbf{b}_{2,3} & \cdots \\ 0 & 0 & \mathbf{b}_{3,2} & 0 & \cdots \\ \vdots & \vdots & \vdots & \vdots & \ddots \end{pmatrix} . \quad (2.20)$$

Each element block of  $\mathbf{b}$  is a matrix with indices  $n$  and  $\mathbf{K}$  implicit,

$$\mathbf{b}_{L,L'} = [[\mathbf{b}_{L,L'}]_{n,n'}(\mathbf{K}, \mathbf{K}')] . \quad (2.21)$$

Using Eqs. (2.8), one finds

$$\begin{aligned}
[\mathbf{b}_{L,L'}]_{n,n'}(\mathbf{K}, \mathbf{K}') &= \delta_{L,L'+1} \sqrt{kT/m} [\delta_{n,n} i(K_x + q_x) + \delta_{n,n'+1} i(K_y + q_y)] \delta_{\mathbf{K}, \mathbf{K}'} \\
&+ \delta_{L,L'-1} \left[ \sqrt{kT/m} [(L+1-n)\delta_{n,n} i(K_x + q_x) + (n+1)\delta_{n,n'-1} i(K_y + q_y)] \delta_{\mathbf{K}, \mathbf{K}'} \right. \\
&\quad \left. + \frac{1}{\sqrt{mkT}} [\delta_{n,n} i(K'_x - K_x) + \delta_{n,n'-1} i(K'_y - K_y)] V(\mathbf{K} - \mathbf{K}') \right]. \quad (2.22)
\end{aligned}$$

Here  $V(\mathbf{K} - \mathbf{K}')$  represents the Fourier component of the adsorption potential  $V(\mathbf{R})$ . The memory function matrix  $\Sigma$  in Eq. (2.15) is diagonal in  $L$  as well as in  $n$  and  $\mathbf{K}$ . Therefore the matrix we need to invert in Eq. (2.7) is block tridiagonal, i.e.,

$$\mathbf{E} = \begin{pmatrix} i\omega & \mathbf{b}_{0,1} & 0 & 0 & \cdots \\ \mathbf{b}_{1,0} & i\omega + \Sigma_1 & \mathbf{b}_{1,2} & 0 & \cdots \\ 0 & \mathbf{b}_{2,1} & i\omega + \Sigma_2 & \mathbf{b}_{2,3} & \cdots \\ 0 & 0 & \mathbf{b}_{3,2} & i\omega + \Sigma_3 & \cdots \\ \vdots & \vdots & \vdots & \vdots & \ddots \end{pmatrix}^{-1}, \quad (2.23)$$

where

$$\begin{aligned}
[\Sigma_L]_{n,n'}(\mathbf{K}, \mathbf{K}') &= [(L-n)\eta_x + n\eta_y] \delta_{n,n} \delta_{\mathbf{K}, \mathbf{K}'} \\
&\times \left[ \theta(\omega_D - \omega) - \frac{i}{2\pi} \ln \left| \frac{\omega - \omega_D}{\omega + \omega_D} \right| \right]. \quad (2.24)
\end{aligned}$$

$$\mathbf{E}_{00} = \left[ -i\omega - \mathbf{b}_{0,1} (-i\omega + \Sigma_1 - \mathbf{b}_{1,2} \{ -i\omega + \Sigma_2 - \mathbf{b}_{2,3} [ -i\omega + \Sigma_3 - \cdots \right. \\
\left. - \mathbf{b}_{L_0, L_0+1} (-i\omega + \Sigma_{L_0+1})^{-1} \mathbf{b}_{L_0+1, L_0} \cdots \}^{-1} \mathbf{b}_{3,2} \}^{-1} \mathbf{b}_{2,1} \}^{-1} \mathbf{b}_{1,0} \}^{-1} \right], \quad (2.27)$$

$$\mathbf{E}_{11} = \left[ -i\omega + \Sigma_1 \frac{\mathbf{b}_{1,0} \mathbf{b}_{0,1}}{-i\omega} - \mathbf{b}_{1,2} \{ -i\omega + \Sigma_2 - \mathbf{b}_{2,3} [ -i\omega + \Sigma_3 - \cdots \right. \\
\left. - \mathbf{b}_{L_0, L_0+1} (-i\omega + \Sigma_{L_0+1})^{-1} \mathbf{b}_{L_0+1, L_0} \cdots \}^{-1} \mathbf{b}_{3,2} \}^{-1} \mathbf{b}_{2,1} \right]^{-1}. \quad (2.28)$$

The continued fraction has to be terminated at some integer  $L = L_0$ . Since  $\Sigma_L$  increases linearly with  $L\eta$ , this continued-fraction expansion is effectively an expansion in inverse powers of the friction parameter  $\eta$ . The termination step  $L_0$  necessary for convergence is larger for smaller values of the friction parameter. It is obvious also from Eqs. (2.27) and (2.28) that the convergence is fastest when  $\omega \gg \omega_0$  [the bare frequency of oscillation in the potential well of  $V(\mathbf{R})$ ] and slowest for small frequencies for a given value of  $\eta$ .

### III. SEPARABLE POTENTIAL

In this section, we first study the case where the adsorption potential has a separable form  $V(\mathbf{R}) = V_0 [\cos(2\pi x/a) + \cos(2\pi y/a)]$  and a fourfold

The correlation matrix  $\mathbf{C} = \chi \cdot \mathbf{E}$ . Since  $\chi$  is diagonal in  $L$ , only the first block ( $L, L' = 0$ ) is needed to evaluate the dynamical structure factor

$$\begin{aligned}
S(\mathbf{q}, \omega) &= \mathbf{C}_{0,0}(\mathbf{K} = 0, \mathbf{K}' = 0; \omega) \\
&= [\rho \cdot \mathbf{E}_{00}](\mathbf{K} = 0, \mathbf{K}' = 0; \omega), \quad (2.25)
\end{aligned}$$

while the second block ( $L, L' = 1$ ) is needed to evaluate the correlation functions  $D_{xx}$  and  $D_{yy}$ ,

$$\begin{aligned}
\mathbf{D}(\omega) &= \mathbf{C}_{1,1}(\mathbf{K} = 0, \mathbf{K}' = 0; \omega)|_{q=0} \\
&= [\rho \cdot \mathbf{E}_{11}](\mathbf{K} = 0, \mathbf{K}' = 0; \omega)|_{q=0}. \quad (2.26)
\end{aligned}$$

$\mathbf{E}_{00}$  and  $\mathbf{E}_{11}$  can be evaluated through a matrix continued-fraction expansion similar to that employed by Risken in the solution of the one-dimensional Fokker-Planck equation.<sup>16</sup> The continued fractions for  $\mathbf{E}_{00}$  and  $\mathbf{E}_{11}$  have the form

symmetry. In this separable potential, the matrix  $\mathbf{b}$  can be decomposed into its  $x$  and  $y$  components,  $\mathbf{b} = b_x \otimes I_y + I_x \otimes b_y$ , where  $I_x$  is the identity matrix in the  $x$  subspace  $I_{mm'}(K_x, K'_x) = \delta_{mm'} \delta_{K_x K'_x}$  and so is  $I_y$  in the  $y$  subspace. Meanwhile,  $\chi$  becomes the outer product  $\chi_x \otimes \chi_y$  and  $\Sigma = \Sigma_x \otimes I_y + I_x \otimes \Sigma_y$ . Therefore the correlation matrix decomposes as

$$\mathbf{C}(\omega) = \int \frac{d\omega'}{2\pi} \mathbf{C}_x(\omega - \omega') \otimes \mathbf{C}_y(\omega'). \quad (3.1)$$

The matrix equation that  $\mathbf{C}_x$  satisfies is similar to Eq. (2.7) but much more tractable:

$$\mathbf{C}_x(\omega) = \chi_x [-i\omega + b_x + \Sigma_x]^{-1}, \quad (3.2)$$

with

$$b_{xmm'}(K_x, K'_x) = \sqrt{kT/m} [\delta_{m,m'+1} + (m+1)\delta_{m,m'-1}] i(K_x + q_x) \delta_{K_x K'_x} + \frac{1}{\sqrt{mkT}} [\delta_{m,m'-1} i(K'_x - K_x) V(K_x - K'_x)], \quad (3.3)$$

$$\Sigma_{xmm'}(K_x, K'_x; \omega) = \eta m \delta_{mm'} \delta_{K_x K'_x} \left[ \theta(\omega_D - \omega) - \frac{i}{2\pi} \ln \left| \frac{\omega - \omega_D}{\omega + \omega_D} \right| \right]. \quad (3.4)$$

The equation for  $C_y$  is identical, with the  $x$  index replaced by  $y$  and  $m, m'$  replaced by  $n, n'$ . The solution of  $C$  is therefore reduced to an effective one-dimensional problem. The inversion of the matrix on the right-hand side of Eq. (3.2) can be achieved through matrix continued-fraction expansion as described in the previous section. However for this case of a separable potential, the algebra simplifies considerably. For the evaluation of  $C_{x(y)}$  we need only to set the index  $n = n' = 0$  ( $m = m' = 0$ ) in Eqs. (2.22), (2.24)–(2.28), which results in much smaller block matrices  $\mathbf{b}, \Sigma$  appearing in the continued-fraction expansion. For this separable potential, we are able to obtain results accurate to better than 1% with the continued fraction terminated at the  $L_0$ -th step [ $L_0 = 10/(\eta/\omega_0)$ ]. We obtain the dynamic structure factors for motion in the  $x$  and  $y$  directions as

$$S_x(q_x, \omega) = C_{x0,0}(K_x = K'_x = 0; \omega), \quad (3.5)$$

$$S_y(q_y, \omega) = C_{y0,0}(K_y = K'_y = 0; \omega). \quad (3.6)$$

The total dynamical structure factor  $S(\mathbf{q}, \omega)$  then follows from Eq. (3.1) as a convolution of  $S_x(q_x, \omega)$  and  $S_y(q_y, \omega)$ ,

$$S(\mathbf{q}, \omega) = \int \frac{d\omega'}{2\pi} S_x(q_x, \omega - \omega') \otimes S_y(q_y, \omega'). \quad (3.7)$$

Qualitatively,  $S_x(q_x, \omega)$  [or  $S_y(q_y, \omega)$ ] has a quasielastic peak centered at  $\omega = 0$  due to the diffusive motion of the adatom, and a peak near  $\omega = \omega_0 \equiv 2\pi/a\sqrt{V_0/m}$  due to the localized adatom vibrational motion near the minima of the adsorption potential. As wave vector increases, the strength of the vibrational peak increases at the expense of the diffusive peak. When the convolution of the  $x$  and  $y$  directions is considered for a wave vector having both  $q_x$  and  $q_y$  components, as in Eq. (3.7), then the full width of the quasielastic peak is given by  $\Delta E(\mathbf{q}) = 2D(q_x^2 + q_y^2)$  for  $q \sim 0$ . However, as  $\mathbf{q}$  increases, the diffusive and vibrational motion are coupled and the quasielastic peak becomes distinctly non-Lorentzian. It can be written in the following form,

$$S(\mathbf{q}, \omega) = \frac{A(\mathbf{q})}{\omega^2 + [\Delta E_D(\mathbf{q})/2]^2} + \tilde{S}(\mathbf{q}, \omega), \quad (3.8)$$

where  $\tilde{S}(\mathbf{q}, \omega)$  is slowly varying near  $\omega = 0$  but peaks at  $\omega$  near  $\omega_0$ .

To illustrate the above discussion, we apply our theory to analyze the Na/Cu(001) system for which He scattering data appeared recently.<sup>8</sup> As argued in Ref. 8, the interaction effects are weak at the experimental Na coverage ( $\theta \sim 0.1$ ) and the adatom motions can be considered as independent. Thus our single-adatom theory is appropriate for the analysis. For this system, the adsorption sites are the fourfold hollow sites. The  $x$  and  $y$  directions correspond to  $[110]$  and  $[\bar{1}10]$  and  $a = 2.56 \text{ \AA}$ . The dynamical structure factor was measured for wave vector  $\mathbf{q}$  along the  $[100]$  direction, and thus it can be factored into the convolution form as described in Eq. (3.7). First,

we focus on the width of the quasielastic peak. Experimentally, an effective  $\Delta E(\mathbf{q})$  was extracted by assuming that the observed data result from the convolution of a Lorentzian with an instrument resolution function. We follow the same procedure to extract an effective  $\Delta E(\mathbf{q})$  from the theoretical value of  $S(\mathbf{q}, \omega)$ . First, we convolute the calculated dynamic structure factor  $S(\mathbf{q}, \omega)$  with an instrumental resolution having a width of  $2w_0 = 0.05w_0$ :

$$S_{\text{eff}}(\mathbf{q}, \omega) = \int \frac{d\omega'}{\sqrt{\pi}w_0} \exp\left[-\frac{(\omega' - \omega)^2}{(2w_0^2)}\right] S(\mathbf{q}, \omega'). \quad (3.9)$$

Then we fit the resultant spectrum  $S_{\text{eff}}(\omega)$  to the convolution of a Lorentzian form with the instrumental resolution function,

$$\int \frac{d\omega'}{\sqrt{\pi}w_0} \exp\left[-\frac{(\omega' - \omega)^2}{(2w_0^2)}\right] \frac{\Delta E(\mathbf{q})A(\mathbf{q})}{\omega'^2 + [\Delta E(\mathbf{q})/2]^2}, \quad (3.10)$$

in the interval  $|\omega| \leq 0.1\omega_0$  to extract an effective FWHM  $\Delta E(\mathbf{q}, \omega)$  for the quasielastic peak. The best fit to the experimental data from Ref. 8 is obtained by choosing the parameters in the Hamiltonian as  $\eta = 0.15\omega_0$  and  $\Delta = 2V_0 = 780 \text{ K}$  (67 meV). The choice of  $V_0$  implies a bare-adatom vibrational frequency  $\nu_0 = \omega_0/2\pi = 1.4 \text{ THz}$ . (This is the frustrated translational mode.) This is considerably less than the Debye frequency for Cu,  $\omega_D/2\pi \approx 7 \text{ THz}$ , and justifies the use of the IVA in the evaluation of  $S(\mathbf{q}, \omega)$ . In Figs. 1 and 2, we plot  $\Delta E(\mathbf{q})$  together with the experimental data taken from Ref. 8 for temperature  $T = 300 \text{ K}$  and  $200 \text{ K}$ , respectively. The theoretical fit of the data is very good. Beyond the first Brillouin zone,  $\Delta E(\mathbf{q})$  increases rather than decreasing to zero toward the center of the second Brillouin zone, as predicted by the multisite jumping theory. This indicates clearly the contribution of the vibrational mode to the quasielastic spectrum. The same conclusion about the importance of the vibrational-motion contribution to the

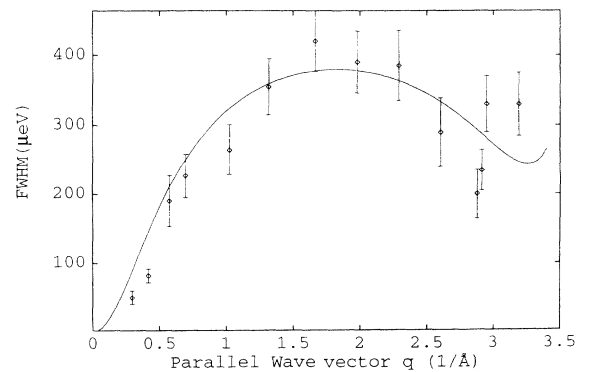


FIG. 1. FWHM ( $\mu\text{eV}$ ) of the quasielastic peak vs the parallel wave vector  $q(\text{\AA}^{-1})$  in the  $[100]$  direction at temperature  $300 \text{ K}$ .  $\eta = 0.15\omega_0, \omega_D = 5\omega_0$ . The solid curve is from the theory. The experimental data with error bars are taken from Ref. 8.

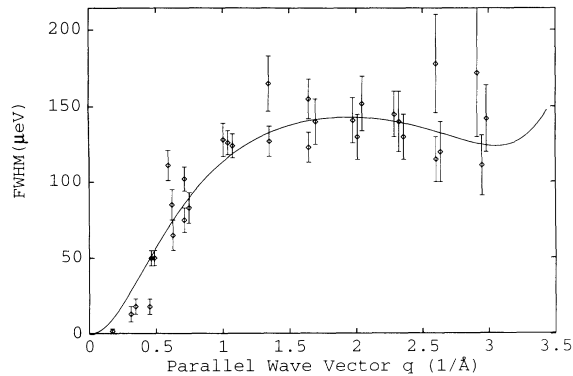


FIG. 2. As Fig. 1, except  $T=200$  K.

quasielastic peak has also been reached via molecular dynamics (MD) simulation studies.<sup>8</sup> We find that, along the  $x$  or  $y$  direction, the behavior of  $\Delta E(\mathbf{q})$  is close to the simple predictions of the multijump theory, without the mixing of diffusive and vibrational motion.

To analyze the microscopic picture of the diffusion, we investigate  $S(\mathbf{q}, \omega)$  in more detail. In Fig. 3, we plot  $S(\mathbf{q}, \omega)$  for  $\mathbf{q}=(1.9\pi/a, 1.9\pi/a)$  and  $T=200$  K. It can clearly be decomposed into a narrow Lorentzian part near  $\omega=0$  plus a more slowly varying part  $\tilde{S}(\mathbf{q}, \omega)$ , as indicated in Eq. (3.8). We extract  $A(\mathbf{q})$  and  $\Delta E_D(\mathbf{q})$  of Eq. (3.8) by a least squares fitting in the frequency range  $0 \leq \omega \leq 0.02\omega_0$ . We then compare  $\Delta E_D(\mathbf{q})$  to the prediction of the multisite jumping model<sup>5</sup>

$$\Delta E_D(\mathbf{q}) = 2\nu \sum_n P_n [2 - \cos(naq_x) - \cos(naq_y)]. \quad (3.11)$$

Here  $\nu$  is the total jumping rate and  $P_n$  the probability for the event of jumping  $n$  sites. In Fig. 4, we plot  $\{P_n\}$  for the two temperatures 200 and 300 K. We note that at both temperatures multiple jumps of two and three steps

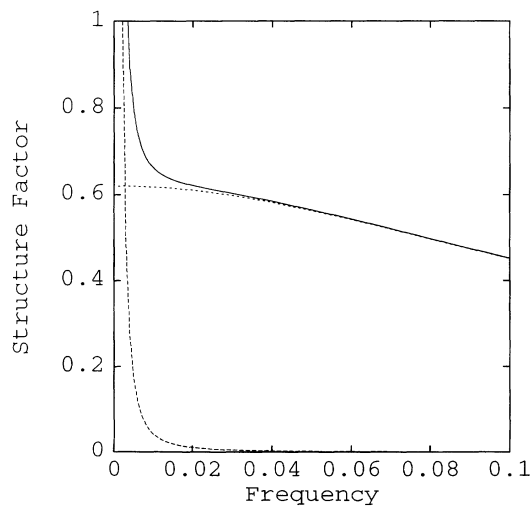


FIG. 3. Dynamic structure factor  $S(q_x=q_y=1.9\pi/a, \omega)$  (scaled with  $1/\omega_0$ , solid curve) decomposed into a sharp Lorentzian peak (dashed curve) and a slowly varying part  $\tilde{S}$  (dotted curve) for  $T=200$  K. The frequency  $\omega$  is scaled by  $\omega_0$ .

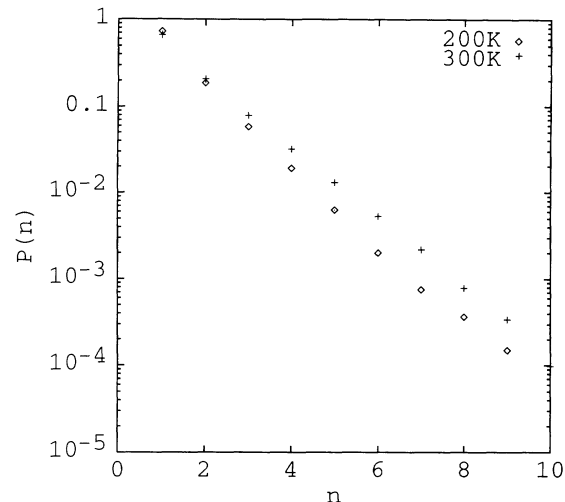


FIG. 4. Jumping probabilities vs jumping distance (in units of the lattice constant).

are frequent. Also the jump rate  $\nu \approx 0.17\nu_0 e^{-\Delta/kT}$  is considerably smaller than the value given by the transition-state theory,  $\nu_{\text{TST}} = \nu_0 e^{-\Delta/kT}$ . This is consistent with the recent theoretical result<sup>9,17</sup> that the probability of multisite jumps increases while the jump rate decreases as  $\eta \rightarrow 0$ . The diffusion constant actually increases as  $1/\eta$  in this limit.<sup>11</sup> Our result for the fraction of double jumps is approximately the same at  $T=200$  K and 300 K, in contrast to that of Ref. 8, which finds a larger fraction of double jumps at  $T=200$  K compared with  $T=300$  K.

The fact that our theoretical result fits the experimental data better than the MD simulation of Ref. 8 can arise from two sources. First of all, the friction parameter  $\eta$  chosen here to be  $0.15\omega_0$  should be considered as an effective friction originating from coupling to all substrate excitations and not just to substrate phonons. In fact, if we use the estimate of  $\eta$  from the continuum elasticity theory,<sup>7</sup>  $\eta/\omega_0$  is found to be only 0.025. Even though this estimate is rather crude, it indicates at least a substantial contribution to the effective friction parameter from coupling to electronic excitations for Na/Cu(001). In the MD simulation, only coupling to substrate phonons is included and this results in an underestimate of  $\eta$ . Secondly, the diffusion constant, or equivalently, the jumping rate, is thermally activated with the Arrhenius form  $Ae^{-\Delta/kT}$ , with  $\Delta$  equal to the diffusion barrier. In our work,  $\Delta=2V_0$  is chosen as 780 K (67 meV). In Ref. 8, the effective barrier is extracted from the maximum broadening at the zone boundary, which contains both vibrational and diffusive contributions and theoretically does not obey a rigorous Arrhenius form. This leads to their choice of a smaller barrier height  $\Delta=51$  meV.

In Fig. 5, we plot the diffusion coefficient  $D_{xx}=D_{yy}=D$  vs friction  $\eta$  for various temperatures. We mention here that the diffusion constant extracted from the curvature of  $\Delta E_D(\mathbf{q})=2D(q_x^2+q_y^2)$  is identical to that given by velocity autocorrelation,  $D_{xx}(\omega=0)$  or  $D_{yy}(\omega=0)$ . At very high temperatures, the adatom is basically executing Brownian motion in a homogeneous viscous medium and

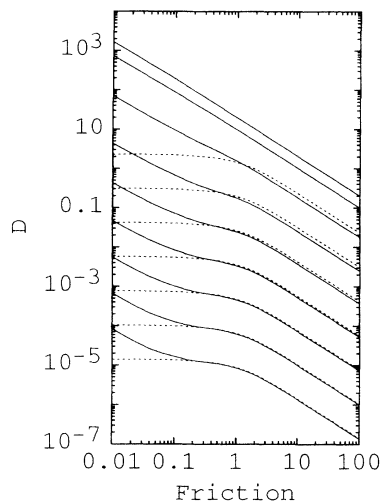


FIG. 5. Diffusion constant  $D$  (scaled by  $\omega_0 a^2$ ) vs friction  $\eta$  (scaled by  $\omega_0$ ) for  $\beta\Delta = 0.02, 0.2, 1$ , and from 3 to 13 by steps of 2 (solid curves, from top to bottom). The dashed lines are for the corresponding Kramers rate theory.

the diffusion constant  $D \simeq kT/\eta$  for arbitrary friction  $\eta$ . As the temperature is lowered, the diffusive motion of the adatom becomes dominated by the thermally activated events of jumping over barriers. Consequently, the temperature dependence starts to conform to the Arrhenius form  $D \propto e^{-\beta\Delta}$  with  $\Delta = 2V_0$  being the barrier height. In the low-temperature region, the diffusive motion can be divided into three regimes corresponding to different values of the friction parameter  $\eta$ . For small friction such that  $\eta \ll \omega_0$ , the rate for the adatom to exchange its energy with the environment is very small. In fact, it vanishes in proportion to  $\eta$ . Although the thermally activated events then become rare, once an adatom is activated with an energy above the barrier, it will travel a distance inversely proportional to  $\eta$  before it relaxes into a potential well. Therefore, the diffusion constant in this regime behaves as  $1/\eta$ . In the opposite limit of high friction,  $\eta \gg \omega_0$ , the adatom is strongly coupled to the environment and exchanges energy with it very rapidly. When an adatom is activated from a potential well and crosses the barrier, it may recross the barrier back to the original well instead of relaxing into the next well. Thus, the diffusion constant is also inversely proportional to  $\eta$  in this limit.<sup>10</sup> Interestingly, for intermediate values of friction, there exists a regime where the diffusion constant is weakly dependent upon friction and is given by the transition-state theory (TST).<sup>4</sup> In this regime, the adatom moves mostly by single-site jumps and there is negligible recrossing of the barrier. In the TST and high-friction regimes, when  $\eta/\omega_0 \geq 1$  and  $\beta\Delta > 2$ , our results compare well with the Kramers rate theory,<sup>18</sup>  $D = (\omega_0 a^2 / 2\pi) (\sqrt{4 + \eta^2 / \omega_0^2} - \eta / \omega_0) e^{-\beta\Delta}$ .

Next we examine the vibrational spectra. In Fig. 6, we plot  $S(q_x = \pi/a, q_y = \pi/a, \omega)$  for various temperatures. At higher temperatures, the vibrational peak is located at the low-frequency side of  $\omega_0$ . The peak becomes sharper as temperature decreases, and its position moves gradual-

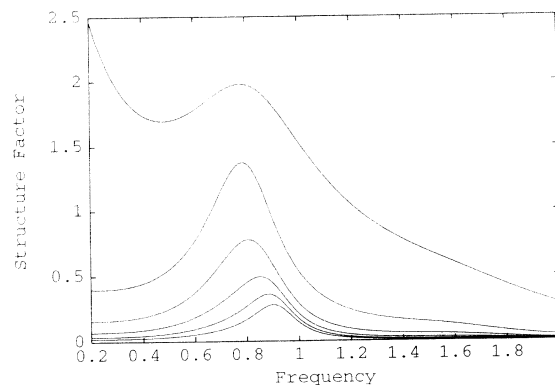


FIG. 6. Vibrational-spectra structure factor  $S(q_x = q_y = \pi/a, \omega)$  (scaled with  $1/\omega_0$ ) for  $T = 780, 512, 300, 200, 180$ , and  $70$  K (from top to bottom); the barrier  $\Delta = 780$  K,  $\eta = 0.15\omega_0$  and  $\omega_D = 5\omega_0$ . The frequency is scaled by  $\omega_0$ .

ly toward  $\omega_0$ . At very low temperatures, the vibrational linewidth is dominated by frictional damping. It is interesting to note that the temperature dependence of the shift of the vibrational peak comes from two different sources. The coupling with substrate excitations tends to shift the peak frequency to the high-frequency end, while the anharmonicity effect pulls it toward the low-frequency side and is dominant for  $\omega_D \gg \omega_0$ . Moreover the anharmonicity-induced line shift has much stronger temperature dependence. At lower temperatures, the anharmonicity effect is smaller and thus the peak position is closer to  $\omega_0$ . Once we have chosen the parameters for the best fit of  $\Delta E(\mathbf{q})$  for the quasielastic scattering peak, the vibrational peak is completely determined in our theory with no further adjustable parameters. Our choice of  $\Delta = 780$  K corresponds to a bare vibrational frequency  $\nu_0 = 1.4$  THz. At  $70$  K, our results indicate a vibrational peak at  $\nu_{70} = 1.35$  THz, while at  $180$  K, the peak is shifted to  $\nu_{180} = 1.22$  THz. These theoretical results are in excellent agreement with the measured values of the frequency of the frustrated translational mode,  $\nu_0 = 1.4$  THz at  $70$  K and  $1.23$  THz at  $180$  K.<sup>8</sup> It would be desirable to have more detailed line-shape analysis of the experimental data for a comparison with our theoretical prediction of the shift and broadening of this vibrational mode.

#### IV. ANISOTROPIC AND NONSEPARABLE POTENTIAL

We now turn to study the vibration and diffusion of an atom adsorbed on an anisotropic surface with a nonseparable potential. The adsorption potential as dictated by the symmetry is modeled by

$$V(\mathbf{R}) = V_0 [1 - \cos(2\pi x/a) \cos(2\pi y/\alpha a)], \quad (4.1)$$

where  $\alpha = \sqrt{2}$ . This potential is appropriate for adsorption on bcc (110) systems, e.g., O/W (110),<sup>19-21</sup> with the coordinates chosen as the  $x$  axis along the  $[1\bar{1}0]$  direction and the  $y$  axis along  $[001]$ . This potential possesses maxima located at  $(x_M = na, y_M = m\alpha a)$  and  $[x_M = (n + 1/2)a, y_M = (m + 1/2)\alpha a]$ , minima at  $[x_m = (n$

$+1/2)a, y_m = m\alpha a]$  and  $[x_m = na, y_m = (m + 1/2)\alpha a]$ , and saddle points at  $[x_S = (n + 1/4)a, y_S = (m + 1/4)\alpha a]$  and  $[x_S = (n + 1/4)a, y_S = (m + 3/4)\alpha a]$ , with  $m, n = 0, \pm 1, \pm 2, \dots$ . The diffusion barrier is determined by the difference between the saddle point and the potential well (the minimum),  $\Delta = V_0$ . For a nonseparable adsorption potential such as that in Eq. (4.1), much more intensive numerical efforts are necessary to evaluate the continued-fraction expansion in Eqs. (2.27) and (2.28). Instead of the full  $S(\mathbf{q}, \omega)$  spectrum for a range of  $\mathbf{q}$  values which was calculated in Sec. III for the separable potential, we have evaluated for this case the velocity autocorrelation function  $\mathbf{D}(\omega)$  for  $\mathbf{q} = 0$ . While  $\mathbf{D}(\omega = 0)$  is directly the diffusion constant, its finite-frequency part carries information about the vibrational modes. It is clear from the form of Eq. (2.17) that, in the IVA, there is a broadening of the adatom vibrational motion due to coupling to the substrate phonon modes whenever  $\omega < \omega_D$ . At the same time, due to the Kramers-Kronig relation for the memory function, the imaginary part of the memory function cause an upward shift of vibrational frequency. This shift is maximum at  $\omega \sim \omega_D$  (in fact, it diverges logarithmically in the IVA). These qualitative features are preserved in the mode-mode coupling approximation, except that  $\text{Re}\Sigma$  is not abruptly cut off at  $|\omega| = \omega_D$  but decays smoothly as  $|\omega| \rightarrow \infty$  due to multiphonon contributions.<sup>11</sup>

Terminating the continued fraction in Eq. (2.28) for  $\mathbf{E}_{11}$  at  $L_0 \equiv (n + m) = 10$  and using  $21 \times 21$  reciprocal lattice vectors, we are able to evaluate  $\mathbf{D}(\omega)$  with an accuracy better than a few percent for values of  $\eta/\omega_0$  between 0.125 and 32. In Fig. 7, we plot the diffusion constants  $D_{xx}$  and  $D_{yy}$  as functions of the friction  $\eta_x = \eta_y = \eta$  for various temperatures. At very high temperatures,  $D_{xx} = D_{yy} \simeq kT/\eta$ . The diffusive motion of the adatom is almost a continuous Brownian motion in a homogeneous, isotropic viscous medium. As the temperature is lowered, the adatom dynamics gradually becomes dominated by thermally activated processes. At very low temperatures, the diffusion proceeds by jump events from one potential well to another via the saddle point. Each jump results in a displacement of the adatom whose projection is  $a$  along the  $x$  direction and  $\alpha a$  along the  $y$  direction; the ratio of the two distances is  $1/\alpha$ . As clearly demonstrated in Fig. 7, the ratio  $D_{xx}/D_{yy}$  approaches the geometric ratio  $1/\alpha^2 = 0.5$ , along with the trend that both  $D_{xx}$  and  $D_{yy}$  get closer to the thermally activated Arrhenius form  $\propto e^{-\beta\Delta}$ . As the value of the friction parameter is varied at low temperatures, we also observe a smooth crossover from the low-friction  $1/\eta$  regime via the TST regime to the high-friction  $1/\eta$  regime. This behavior is exactly parallel to the discussion we have presented in Sec. III for the separable potential.

In Figs. 8–10, we plot the dynamic correlation function  $\mathbf{D}(\omega)/kT$  for  $\eta/\omega_0 = 0.1$  and  $\omega_D = 3\omega_0$  at various temperatures. For this relatively low friction value, the matrix continued fraction is still terminated at  $L_0 = 10$  and thus the low-frequency part of  $\mathbf{D}(\omega)$  may not be reliable, whereas the vibrational part should be qualitatively correct since the convergence of the continued fraction improves with increasing  $\omega$ . Let us first analyze  $D_{xx}(\omega)$ .

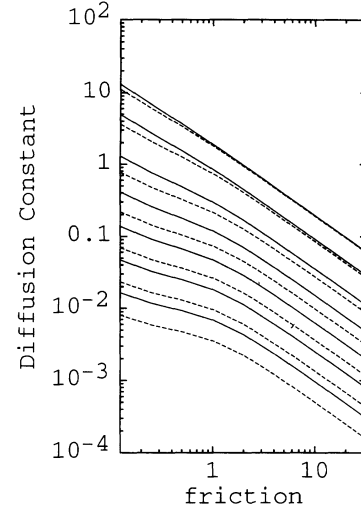


FIG. 7. Diffusion constants (scaled by  $\omega_0$ )  $D_{xx}$  (dashed lines) and  $D_{yy}$  (solid lines) vs friction coefficient  $\eta$  (scaled by  $\omega_0$ ) for  $\beta\Delta = 0.5 - 6.5$  by steps of 1 (from top to bottom).

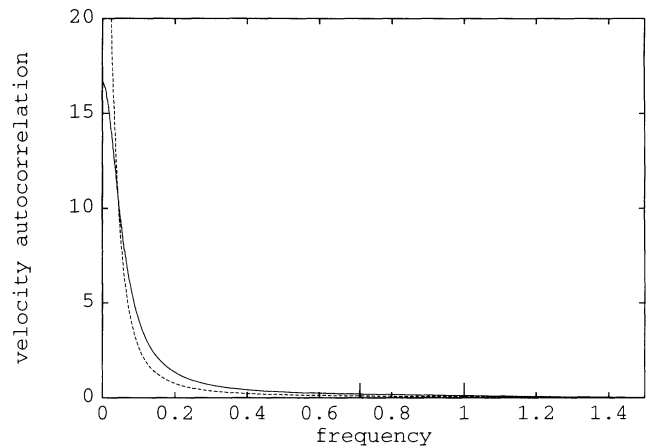


FIG. 8.  $D_{xx}(\omega)/kT$  (scaled by  $1/\omega_0$ , solid line) and  $D_{yy}(\omega)/kT$  (scaled by  $1/\omega_0$ , dashed line) vs frequency  $\omega$  (scaled by  $\omega_0$ ) for  $\beta\Delta = 0.5$ . The position of  $\omega_{0x} = \omega_0$  and that of  $\omega_{0y} = \omega_0/\sqrt{2}$  are marked with long ticks on the frequency axis.

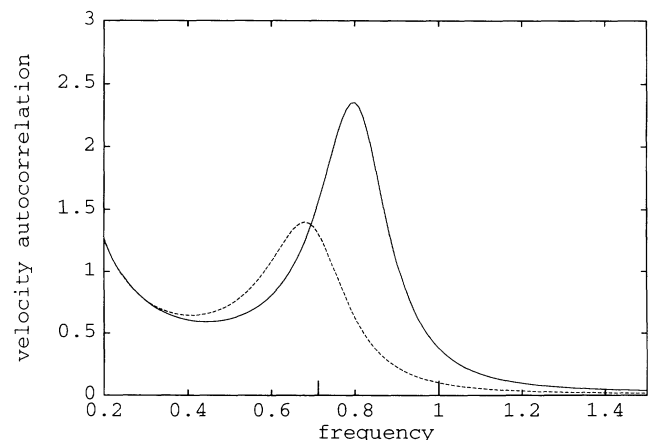


FIG. 9. As for Fig. 8 except that  $\beta\Delta = 1.5$ .

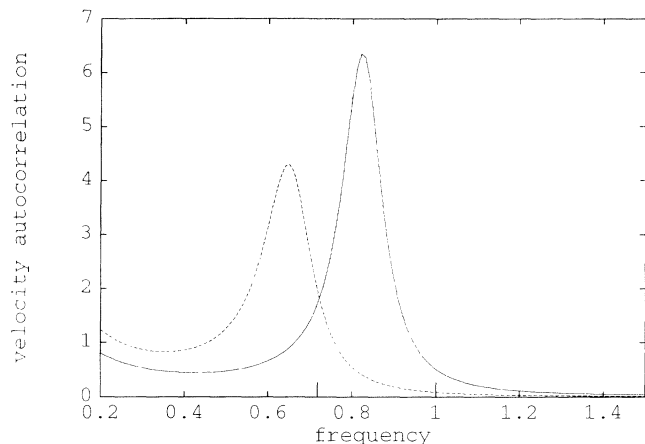


FIG. 10. As for Fig. 8 except that  $\beta\Delta=2.5$ .

At high temperatures, when  $\beta\Delta < 1$ , it possesses a prominent diffusive peak at low frequency  $|\omega| \sim 0$  and it is nearly structureless at the vibrational frequency  $\omega \sim \omega_{0x} \equiv \omega_0$ . At the temperature decreases, the diffusive peak is suppressed and the vibrational peak gains weight accordingly. The line shape of the vibrational peak is asymmetrical with stronger broadening on the low-frequency side. Moreover it is shifted to the low-frequency side of the bare frequency  $\omega_{0x}$ . While the vibrational peak becomes sharper as the temperature is lowered, its position moves gradually toward  $\omega_{0x}$ . At very low temperatures, the vibrational linewidth is dominated by the friction coefficient  $\eta$  which results from collisions with phonons. As in the case of a separable potential, the coupling with substrate phonons tends to shift the peak frequency to the high-frequency end, whereas the anharmonicity effect pulls it toward the low-frequency to the high-frequency end, while the anharmonicity effect pulls it toward the low-frequency side and is dominant for  $\omega_D \gg \omega_0$ . Moreover the anharmonicity-induced line shift has a much stronger temperature dependence. The anharmonicity effect is smaller at lower temperatures and thus the peak position is closer to  $\omega_{0x}$ . The line shapes of the vibrational modes in  $D_{yy}(\omega)$  are also asymmetrical. The peak of  $D_{yy}(\omega)$  is shifted toward the low-frequency side of  $\omega_{0y} \equiv \omega_0/\sqrt{2}$ . The shift in the position of the  $D_{yy}(\omega)$  peak, however, is more complicated than the corresponding behavior for  $D_{xx}(\omega)$ . The anharmonicity within the  $y$  mode tends to shift the peak toward the low-frequency side of  $\omega_{0y}$ . However, anharmonicity also causes the mixing of the  $y$  mode with the  $x$  mode and thus shifts the  $y$  mode in the opposite direction because  $\omega_{0x} > \omega_{0y}$ . The  $y$ -mode shift therefore has a non-monotonic temperature dependence. At  $\beta\Delta=1.5$ , the two frustrated translational modes are strongly

broadened and they almost overlap. As the temperature decreases to  $\beta\Delta=2.5$ , the  $y$  mode is gradually decoupled from the  $x$  mode and the  $y$  peak shifts toward the low-frequency end.

## V. CONCLUDING REMARKS

We have presented a microscopic theory of diffusion and vibration of an adatom on solid surfaces. For a separable potential, we evaluated and analyzed the dynamic structure factor. When applied to the Na/Cu(001) system with a fourfold symmetry, the calculated full width at half maximum of the quasielastic spectrum and the shifted vibrational frequency are in excellent agreement with the experimental data from He scattering experiments. The quasielastic scattering spectrum is demonstrated to have contributions from the vibrational as well as from the diffusive modes. The contribution of both the anharmonic potential and frictional damping to the adatom vibrational spectrum are also discussed in detail. We have also investigated the vibrational spectra and diffusion constant of an adatom on an anisotropic system such as a bcc (110) surface with a nonseparable adsorption potential by evaluating the velocity autocorrelation function of the adatom. The temperature dependence of the diffusion constant clearly demonstrates a smooth crossover from the high-temperature continuous Brownian motion behavior to the low-temperature thermally activated characteristics. As the friction is varied at low temperatures, one also observes the change from the low-friction multisite jumping regime to the transition-state regime and then to the high-friction overdamped regime. The frequency spectra of the velocity autocorrelation function show the broadening and shift of the vibrational modes. At temperatures higher than the diffusion barrier, the spectra have only a diffusive peak at  $|\omega| \sim 0$  with no detectable trace of vibration. At temperatures comparable with the barrier height, the vibrational linewidth is dominated by anharmonic dephasing. At temperatures much lower than the barrier height, frictional coupling with substrate excitations becomes the dominant dephasing factor. Since the bare frequencies of the two frustrated translational modes for the anisotropic surface are different from each other, the temperature dependence of the shift of the vibrational modes is considerably more complicated than for the surface of fourfold symmetry.

## ACKNOWLEDGMENTS

We thank Tapio Ala-Nissila for many helpful discussions. This work was supported in part through an ONR grant.

<sup>1</sup>R. Gomer, Rep. Prog. Phys. **53**, 917 (1990).

<sup>2</sup>A. Laubereau and W. Kaiser, in *Chemical and Biological Applications of Lasers*, edited by C. B. Moore (Academic, New York, 1977), Vol. II.

<sup>3</sup>S. Marks, P. A. Cornelius, and C. B. Harris, J. Chem. Phys. **73**,

3069 (1980).

<sup>4</sup>G. H. Vineyard, Phys. Rev. **110**, 999 (1958).

<sup>5</sup>C. T. Chudley, and R. J. Elliott, Proc. Phys. Soc. London **77**, 353 (1961).

<sup>6</sup>J. W. Gadzuk and A. C. Luntz, Surf. Sci. **144**, 429 (1984).

- <sup>7</sup>B. N. J. Persson and R. Rydberg, *Phys. Rev. B* **32**, 3586 (1985).
- <sup>8</sup>J. Ellis and J. P. Toennies, *Phys. Rev. Lett.* **70**, 2118 (1993); *J. Electron Spectrosc. Relat. Phenom.* **64** (1993).
- <sup>9</sup>R. Ferrando, R. Spadacini, and G. E. Tommei, *Phys. Rev. E* **48**, 2437 (1993); *Surf. Sci.* **265**, 273 (1992).
- <sup>10</sup>S. C. Ying, *Phys. Rev. B* **41**, 7068 (1990); T. Ala-Nissila and S. C. Ying, *Prog. Surf. Sci.* **39**, 227 (1992).
- <sup>11</sup>L. Y. Chen and S. C. Ying, *J. Electron Spectrosc. Relat. Phenom.* **64**, 797 (1993).
- <sup>12</sup>L. Y. Chen and S. C. Ying, *Phys. Rev. Lett.* **71**, 4361 (1993).
- <sup>13</sup>The vertical motion of the adatom only serves to renormalize the parameters in the Hamiltonian for the study of diffusion and lateral vibrations.
- <sup>14</sup>H. Mori, *Prog. Theory. Phys.* **34**, 399 (1965).
- <sup>15</sup>G. Wahnström, *Surf. Sci.* **159**, 311 (1985).
- <sup>16</sup>H. Risken, *The Fokker-Planck Equation* (Springer, Berlin, 1989).
- <sup>17</sup>E. Pollak, J. Bader, B. J. Berne, and P. Talkner, *Phys. Rev. Lett.* **70**, 3299 (1993).
- <sup>18</sup>H. A. Kramers, *Physica (Utrecht)* **7**, 284 (1940).
- <sup>19</sup>M. Tringides and R. Gormer, *Surf. Sci.* **155**, 254 (1985).
- <sup>20</sup>M. Tringides and R. Gormer, *Surf. Sci.* **166**, 419 (1986).
- <sup>21</sup>J. Kjoll, T. Ala-Nissila, and S. C. Ying, *Surf. Sci.* **218**, L476 (1989).